Low Temperature Loss Measurement of Aluminium Thin Film Transmission Lines

Pooja Singh[a,b], Sandhya M Patel[a,b*] & P K Siwach[a,b]

[a]CSIR-National Physical Laboratory, Dr. KS Krishnan Marg, New Delhi 110 012, India
[b]Academy of Scientific and Innovative Research (AcSIR), Ghaziabad 201 002, India

In this article, we study the planar microwave structures made from Aluminium thin films deposited by the sputtering technique at low temperature. The loss mechanisms in these Aluminium transmission lines deposited on Silicon substrates have been analysed by considering the stopping distance in the conducting lines. It is shown that the attenuation of the lines depends on the material properties and edge shape of the transmission lines. The two-port microwave transmission measurement of the structures was performed with a vector network analyser in the 1-12 GHz frequency range using a cryostat system. This work presents that Aluminium can be a potential candidate for various applications, namely MKIDS, and can replace other conventional superconductors for low temperature applications. Additionally, stopping distance analysis in silicon substrate-based microstrip lines can be continued in order to analyse the precise losses due to the step edge fabrication of the transmission lines. This analysis can then be used to estimate the uncertainty in the loss measurement. This work will be beneficial for developing the transmission lines for a variety of cutting-edge technologies, including quantum computing, the Internet of Things, and high-speed communication systems, where loss parameters play a crucial role.

1 Introduction

Transmission lines either fabricated from metallic (conventional) or superconducting materials are widely used in microwave systems appropriate for operations up to 300 GHz[1–3]. Owing to the ease of their fabrication, these have been widely used as passive and active components in various microwave applications. Over the last few decades, these have evolved as integral components in classical engineering and modern physics. The microwave absorption in thin metal films has been studied using a variety of resonator techniques[4-5], but there has also been interest in the theory of the absorption of thin metal films[6-7]. However, these theories are appropriate for typical incident plane waves but cannot be applied to the loss estimates[8].

For the purpose of calculating the conductor loss of a microwave transmission line structure, a number of field theoretic methods, such as the quasi-TEM method[9], spectral domain analysis[10,11], mode matching methods[12], *etc*., have been reported. Wheeler's incremental inductance rule is also used for this purpose, although this method is only applicable to the conductor thickness more than the skin depth[13]. A few models are reported to determine the conductor loss of a coplanar waveguide (CPW) for the conductor thickness less than three times the skin depth which is mainly used in MMIC technology[14-17].

However, low-loss microwave circuit components have always been crucial for emerging superconducting quantum-based technologies. The microwave passive components, like CPW-based resonators, are the critical elements for kinetic inductance, superconducting quantum bits and quantum memories, and various microwave nano-mechanical experiments[18-19]. Superconducting transmission lines are extremely desired for high-speed electronics due to their absence of dispersion[20-22], which is what led to the development of successive generations of superconducting electronics and digital computing starting in the 1970s[23]. As the transmission line observes the TEM mode of propagation, the superconducting transmission line is dispersion-less because the penetration depth does not change with frequency. This is in contrast to a normal conductor

———————
*Corresponding author:
(E-mail: patelsm@nplindia.org)

case, where the internal conductance decreases with increasing frequency and the skin depth of the metal conductor varies inversely with frequency. Superconductors are thus used instead of conventional ones for a variety of applications since they have low losses when used in transmission lines.

Although employing superconductors as a transmission line has a number of benefits over using normal conductors, the loss estimates for superconducting transmission lines (STLSs) call for explicit considerations. The thickness and the cross-section of the conducting lines usually differ from the intended or expected shape. The fabrication process heavily influences the geometry of the metal conductors, which frequently results in a trapezoidal shape rather than the optimum rectangular shape. The modified matched asymptotic expansion technique[24-25] has been used to calculate the attenuation and other parameters for such deviated forms in the transmission lines. The stopping distance is defined as the trapezoidal form or the brief distance before the edge[30]. In STLs also, this stopping distance has been considered and studied by Booth[26]. The conductor losses have been calculated depending on the penetration depth and the normal skin depth and also the shape of the conducting line. High-performance passive microwave components made of a variety of superconducting materials are currently being used oftentimes[27]. They have taken the place of their traditional counterparts, like filters in wireless communication networks. It is now possible to create multiple superconducting microwave components in planar structures because high-quality superconducting thin films can now be produced. The two most often utilised components in microwave applications are superconducting microstrip and coplanar lines. In order to compute the loss parameters of these transmission lines at high frequencies with harmonics well into the microwave zone, correct modeling and perturbation methods are very necessary. Booth has thought about and researched this stopping distance in STLs as well[26]. According to the penetration depth, the depth of the normal skin, the conducting line's shape, and other factors, the conductor losses have been determined.

The microwave losses in Aluminium (Al) thin film structures fabricated on silicon substrate measured at liquid helium temperature were the emphasis of this study. Aluminium has a self-limiting oxide and a low loss at microwave frequencies, which makes it a potential material for superconducting devices[28]. Earlier studies have demonstrated that aluminium thin film with granular properties[29] were useful for high kinetic inductance and low-loss quantum devices as these are secured from flux-noise-induced decay and dephasing. Also, for the operation of quantum devices like superconducting qubits, whose frequency normally does not exceed 10 GHz, the superconducting gap in Al, (*i.e.*, $\approx$ 100 GHz), is sufficient. Aluminium, which serves as the main component of superconducting electronics, can be considered analogous to Silicon (Si), which performs a similar function in semiconductor electronics. The suitability of this substrate for the manufacture of STLs particularly for the usage of electronic components, had already been established in earlier reports[30-33]. Since, superconductors are ideal lossless materials, the loss tangent of this substrate is crucial in regulating the line's overall loss. In order to streamline the device analysis and narrow the focus to the external system loss originating from the external circuitry, a low value is used[34]. Although Al and Si, as superconductors or semiconductors, have certain limits, these drawbacks are offset by the exceptional qualities of their oxides. The growth of Al thin films on the Si substrate had been optimised and studied extensively[35-36] to show excellent results favouring to realize devices for Josephson tunnel junctions and HEB devices consisted of narrow micro bridges for space applications. Various earlier studied[37-41] have also supported the fact that the Al metallization on Si can be used for microelectronics technology. The understanding required for microwave active devices with superconducting properties and applications at THz frequency is aided by knowledge of the interaction effects between Al and Si[42].

In this paper, we provide the results of loss investigations on Al transmission lines fabricated on Si substrates and tested at frequencies up to 12 GHz. The losses measured at room and low temperatures, as well as the calculated loss using the stopping distance concept, are also compared. We finish with a discussion of the approach's limitations for calculating conductor loss in superconducting planar circuits.

2 Proposed Theory

The Al transmission lines were measured at microwave frequency both at an ambient temperature (25°±2 °C) and at low temperature of liquid Helium (4.2 K). The two-port microwave measurements of

the Al lines were performed with a vector network analyser (VNA) measurement system using model N5227A PNA. An indigenously designed sample holder was developed to fix the Al lines between the two measurement ports of the flexible cables. This sample holder (schematics shown in Fig. 1(a) & 1(b) has been fabricated using OFHC copper as it is corrosion free and highly thermal conductive. This developed sample holder has the provision of linear and vertical adjustments to incorporate the sample of different dimensions. The two-port microwave measurements of superconducting thin films and nanostructures at low temperatures have been carried out successfully using this sample holder

The VNA was first calibrated using the simple SOLT (Short, Open Load, Thru) method. The reference planes of the VNA were joined together to create a through connection once all the procedures of connecting each standard at the reference planes were finished. This connection was used for the final measurements of the samples to get the respective scattering parameters (S-parameters) using VNA. The S parameters of the Al transmission lines were then measured up to the 12 GHz frequency band and saved for the subsequent RLGC parameter calculations based on the extraction method[43].

The transmission line parameters are extracted from the S-parameter characterisation of the lines using the Eqs. (1) and (2).

$$e^{-\gamma l} = \frac{2S_{21}}{1 - S_{11}^2 + S_{21}^2 \pm \sqrt{\left(1 + S_{11}^2 - S_{21}^2\right)^2 - 4S_{11}^2}} \qquad \ldots (1)$$

$$Z_c = \pm Z_o \sqrt{\frac{(1 + S_{11})^2 - S_{21}^2}{(1 - S11)^2 - S_{21}^2}} \qquad \ldots (2)$$

where, Z_o is 50 ohm, S_{11} and S_{21} are the S-parameter responses of the line, and l is the length of the finite transmission line and γ is the propagation constant and Z_c is the characteristic impedance. Once the Z_c and γ are defined, then from the standard transmission line relationships given in Eqs. (3) and (4):

$$\gamma = \sqrt{(R + j\omega L)(G + j\omega C)} \qquad \ldots (3)$$

$$Z = \sqrt{\frac{(R + j\omega L)}{(G + j\omega C)}} \qquad \ldots (4)$$

Then,

$$R = Re(\gamma Z_c) \qquad \ldots (5)$$

$$L = \frac{Im(\gamma Z_c)}{\omega} \qquad \ldots (6)$$

$$G = Re\left(\frac{\gamma}{Z_c}\right) \qquad \ldots (7)$$

$$C = \frac{Im\left(\frac{\gamma}{Z_c}\right)}{\omega} \qquad \ldots (8)$$

Thus, the Telegrapher's equation transmission line model parameters are determined by combining (5)-(8). Here, R, L, G and C are referred to as resistance, inductance, conductance, and capacitance per unit length of the line. It was studied that R and G losses are caused by dielectric substrate loss and the action of quasi-TEM waves propagating above the conducting strip. As a result, the frequency-dependent attenuation may be derived from the predicted Z_c, R, L, and G. As a result, attenuation (α) relies mainly on R and G, allowing for the calculation of total attenuation using R & G as shown in Eqs. (9) and (10) below

$$\alpha = \alpha_R + \alpha_G \qquad \ldots (9)$$

$$\alpha = \frac{R}{2Z_c} + \frac{GZ_c}{2} \qquad \ldots (10)$$

Where, α_R is the attenuation due to conductor loss, and α_G is attenuation due to the dielectric loss.

Now to determine the conductor loss for superconducting planar structures, the stopping distance Δ is determined for a given edge shape as a function of conductor thickness t, and skin depth δ which was determined using the asymptotic expansion of the fields local to the edge which was characterized by the power loss of an arbitrary shaped edge as in[15]. Once the stopping distance Δ is determined, the attenuation constant of the microstrip line of width W is calculated using Eqs. (11)
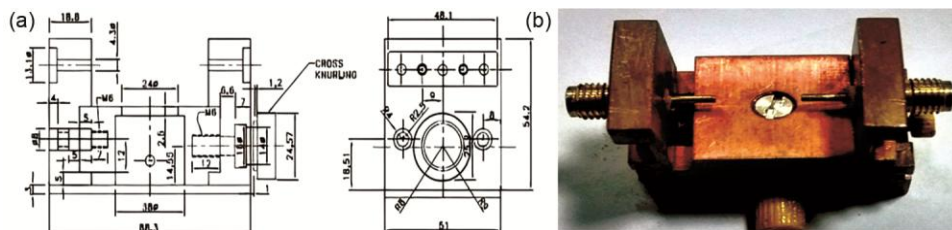
Fig. 1 — (a) Schematic of the sample holder (b) Developed 2-port sample holder.

$$\alpha = \frac{R_{sm}}{2\pi^2 Z_o} \frac{\ln\left(\frac{W}{\Delta}-1\right)}{W} \qquad \ldots (11)$$

Here, R_{sm} is the modified surface impedance for a superconductor strip of thickness t given by (12)

$$R_{sm} = \mu_o \omega t Im \left(\frac{cot(k_c t) + csc(k_c t)}{k_c t}\right) \qquad \ldots (12)$$

where, k_c is the complex wavenumber in the superconductor at a frequency ω given by (13)

$$k_c = \left(\frac{1}{\lambda}\right)^2 + 2i\left(\frac{1}{\delta_{nf}}\right)^2 \qquad \ldots (13)$$

Here, δ_{nf} is the normal fluid skin depth and λ is the superconducting magnetic penetration depth.

In this way, we proposed a simple method to find the characteristic loss parameters of the Al transmission lines fabricated on Si substrate.

3 Experimental Methods

3.1 Material Preparation

To fabricate the transmission line structures, the thin shadow mask, using a sheet of invar steel of thickness 0.018 mm (shown in Fig. 2(a) & (b), was prepared with the help of CNC (computer numerical control) machine. By using this mask and a magnetron sputtering setup with a 30 W dc power, Al thin films deposited on Si (100) substrates with a dielectric constant of 11.9. The proper ultrasonicate cleaning of the mask was followed beforehand. Before deposition, the base vacuum of the sputter-chamber was maintained at 9×10^{-7} mbar. The films were deposited from 2-inch commercially procured Al target (American Elements) under 5N pure Argon gas pressure of 6.7×10^{-3} mbar at room temperature. The target to substrate distance was fixed at 5 cm and the deposition time was 5 mins. The thickness of the

commercially available Si wafer used is 0.3 mm and 100 nm thin Al film is obtained by sputter deposition. The optimal rate of deposition was used to determine the thickness of the Al films. To determine the deposition rate, the thickness of the various films deposited under varied growth conditions was measured using a stylus profilometer. The stylus profilometer's step height measurement was utilized to calculate the thickness of the deposited films.

3.2 Microwave Characterization

For S-parameter measurements using the VNA system, the Al transmission lines were positioned securely between the two ports of the fixture. The fixture connectors were connected to the flexible cryocables for the S-parameter measurements using the calibrated VNA. The same arrangement was used to measure the samples at room temperature and at liquid helium temperature as well. For the low temperature measurements, the flexible cryo-cable-attached fixture was simply dipped into the cryostat system with the help of the two additional cryocables. These cryocables are robust, flexible, and have a low insertion loss to meet the requirement of microwave measurements at low temperatures. Using VNA, the S-parameters were measured at both ambient and liquid temperatures.

4 Results and Discussion

The Aluminium transmission lines were first designed to have the desired characteristic and then simulated using HFSS 3D simulator. The schematic model of one of the transmission line structure with the HFSS software is shown in Fig 3. The thickness of the Al was 100 nm fabricated on the Si substrate ($\varepsilon_r = 11.9$) of thickness 300 μm. The width of the centre line was 0.25 mm. The Al/Si microstrip line
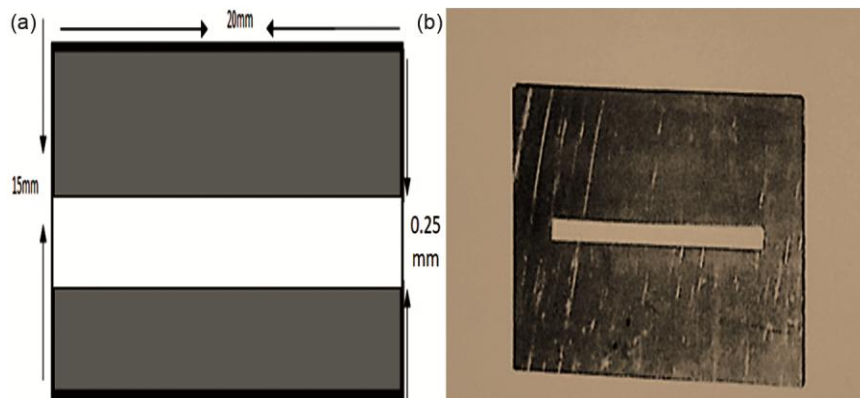
Fig. 2 — (a) Layout of the mask (b) Developed mask for the fabrication of the microstrip line.

structure was simulated using HFSS up to 12 GHz to get the S_{11} and S_{21} as shown in Fig 4.

A similar structure with Aluminium on a Si substrate was fabricated using the sputtering technique. The structures were first measured at room temperature and then at liquid helium temperature (*i.e.*, at 4.2 K). The measured S-parameter responses of the structure measured at room temperature and liquid helium temperature are given in Fig 5.

The measured S-parameters (shown in Fig. 5) make it amply obvious that the transmission line exhibits reduced losses and improved conductivity at microwave frequencies when measured at low temperature. The transmission parameter (S_{21}) shown in Fig. 5 (right side) showed an abundant improvement of 0.4 dB at low temperature. Similar conclusions can be drawn from the measured S_{11} parameters for both temperature conditions. The transmission line exhibits a noticeable improvement of about 20 dB at lower frequencies upto 8 GHz when measured at low temperature, but the reflection loss slightly increases at higher frequencies upto 12 GHz. At frequencies between 10 GHz to 12 GHz, we found some fluctuations in the return loss (S_{11}) measurements which may be caused by interference

Fig. 3 — Structure of the microstrip line designed on HFSS simulator
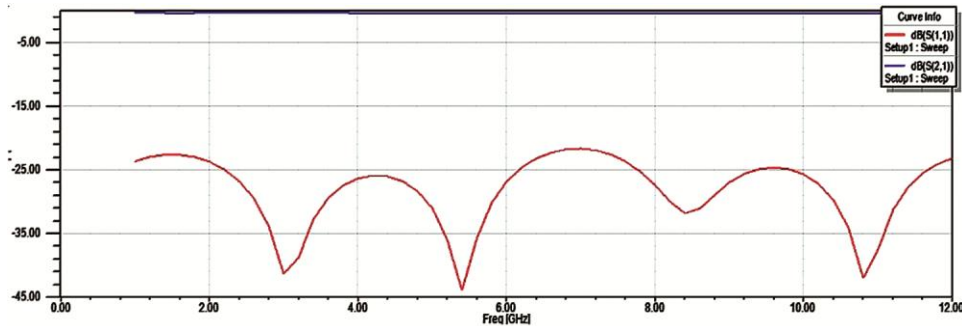
Fig. 4 — Simulated S parameter (S_{11} and S_{21}) for the Al/Si microstrip line structure
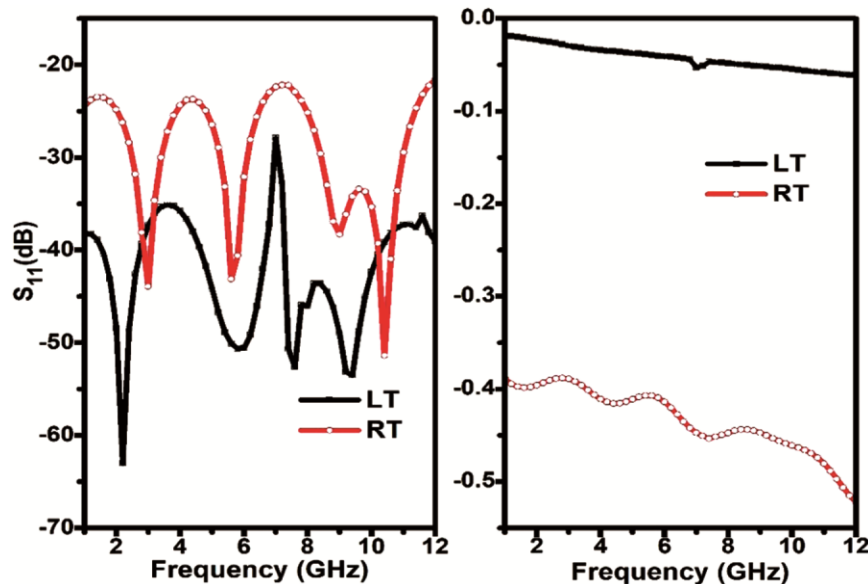
Fig. 5 — Measured S_{11} and S_{21} of the Al/Si structure at room temperature (shown as RT) and at liquid Helium (shown as LT)

in the cryostat system used for the low temperature measurement instrument. Hence, it is apparent that aluminium transmission lines exhibit better transmission performance at low temperatures than at normal temperatures when measured at microwave frequency upto 12 GHz. This information encouraged and prompted more investigation into the loss mechanisms in superconducting transmission lines in order to understand their usefulness in digital applications.

The RLGC parameters were extracted as described in section 2 based on these S-parameter results for both the room temperature and low temperature. These RLGC parameters finally provide different losses of the transmission lines. In a transmission line structure, the losses depend on the nature of conducting material used in the strip conductor, the material of the substrate and ground plane, and the physical structure of the conducting line. The total loss in a line structure commonly occurs due to the dissipative effects, *i.e.*, conductor loss and dielectric loss and the parasitic phenomenon leading to radiation loss. The conductor loss is caused mainly by the finite conductivity of the strip conductor and the ground plane conductor if used, whereas the dielectric loss is contributed by an imperfect lossy substrate material. For frequencies above 200 GHz, total attenuation is usually dominated by radiation loss, so the effect of radiation losses has been neglected in this work. The graph plotted as Fig. 6 depicts the comparison plot for aluminium microstrip lines measured at low and room temperatures conditions.

The plots in the above graph of various losses for the aluminium structure recorded at two temperature levels clearly reveal that both the conductor and dielectric losses in the aluminium structure were comparatively low at low temperatures as compared to room temperature data. At room temperature, the conductor loss was less than -5 dB and the dielectric loss was less than -1 dB, resulting in an overall attenuation of less than -3 dB for the whole frequency range. On the other hand, when measured at liquid helium temperature, the same structure has substantially reduced loss characteristics. At low temperatures, there is a 3 dB improvement in the conductor loss, and the dielectric loss is also decreased by 10 dB, for an overall loss reduction of 5 dB.

The conductor loss of the same structure has been computed using the standard perturbation method along with the concept of the stopping distance Δ. The perturbation expression to compute the conductor loss of the structure is already explained in section 2. The intricacy of applying this calculation to the superconducting materials is the fact that two material parameters are needed to be specified to determine the stopping distance Δ from[15] which in contrast to the case of normal metal conductors, which require only one material parameter. The graph presented in Fig. 7 compares the transmission line loss measured at low temperature with the calculated conductor loss taking the stopping distance into consideration. Examining the charts, it is obvious that the computed loss with stopping distance is nearly identical to the actual loss at low temperatures up to the specified frequency of 8
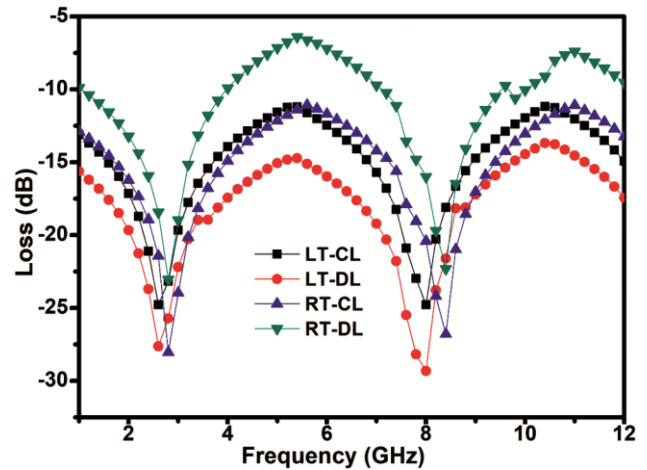
Fig. 6 — Losses (in dB) computed from measured S_{11} and S_{21} of the Al/Si structure at room temperature (shown as RT) and at liquid Helium (shown as LT), CL denotes the conductor loss and DL denotes the dielectric loss.
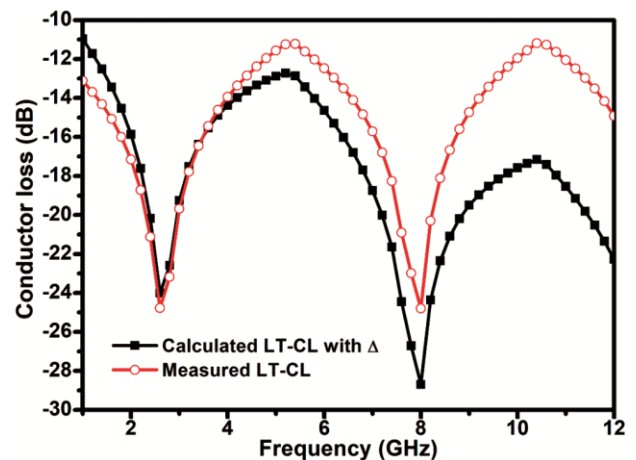
Fig. 7 — Comparison of the measured low temperature conductor loss with the calculated loss taking stopping distance into consideration.

GHz, but the deviation becomes noticeable at higher frequencies. This deviation could be the result of the dipole coupling from an unbalanced current flowing normal to the surface of the conductor at higher frequencies. However, this approach can be useful in determining the exact losses when designing the transmission line structures at low temperature applications.

5 Conclusion

Planar transmission lines for low-temperature microwave circuits have been designed and developed. We have presented closed-form expressions, which are based on a calculation of the stopping distance, for the attenuation constant due to conductor loss for the Al transmission lines structure. This work can be expanded to include the use of aluminium as a thin film microwave structures for a variety of low temperature components. In the future, we will investigate more precise methods of computing the overall loss performance of the microwave circuit with de-embedding process.

Acknowledgment

References

1   Dehe A, Klingbeil H, Weil C & Hartnagel G L, *IEEE Microw Guided Wave Lett*, 8 (1998) 185.
2   Ponchak G E, Matloubian M & Katehi L P B, *IEEE Trans Microw Theory Tech*, 47 (1999) 241.
3   Rastogi A K & Mishra S, *Int J Infrared Millim Waves*, 20 (1999) 505.
4   Zychowicz T, Krupka J & Mazierska J, *Proc APMC*, (2006) 572.
5   Sun X, *Proc Int Conf Microwave Millim Wave Tech*, (2008) 624.
6   Gopinath A, *IEEE Trans Microw Theory Tech*, 30 (1982) 1101.
7   Schollhorn C, Zhao W, Morschbach M & Kasper E, *IEEE Trans Electron Devices*, 50 (2003) 740.
8   Ramey R L & Lewis T S, *J Appl Phys*, 39 (1968) 1747.
9   Heinrich W, *IEEE Trans Microwave Theory Tech*, 41 (1993) 45.
10   Ke J Y & Chen C H, *IEEE Trans Microwave Theory Tech*, 43 (1995) 1128.
11   Kitazawa T & Itoh T, *IEEE Trans Microwave Theory Tech*, 39 (1991) 1694.
12   Heinrich W, *IEEE Trans Microwave Theory Tech*, 38 (1990) 1468.
13   Verma A K, Nasimuddin & Singh H, *Proceedings of APMC*, China, 2004.
14   Holloway C L & Kuester E F, *Radio Sci*, 29 (1995) 539.
15   Holloway C L & Kuester E F, *IEEE Trans Microwave Theory Tech*, 43 (1995) 2695.
16   Holloway C L, *Microwave Opt Tech Lett*, 25 (2000) 162.
17   Ponchak G E, Matloubian M & Katehi L P B, *Int J Microcircuits Elect Pack*, 20 (1997) 167.
18   Cicak K, Li D, Strong J A, Allman M S, Altomare F, Sirois A J, Whittaker J D, Teufel J D & Simmonds R W, *Appl Phys Lett*, 96 (2009).
19   Gu X, Kockum A F, Miranowicz A, Liu Y X & Nori F, *Phys Rep*, 718 (2017) 1.
20   Kautz R L, *J Appl Phys*, 49 (1978) 308.
21   Matick R E, *Lines for Digital and Communication Networks*, IEEE Press, 1995.
22   Ekholm E B & McKnight S W, *IEEE Trans Microw Theory Tech*, 38 (1990) 387.
23   Anacker W, *IBM J Res Develop*, 24 (1980) 107.
24   Bromme R & Jansen R H, *IEEE MTT-S Int Microwave Symp Dig*, 3 (1991) 1081.
25   Dib N I, Harokopus W P J, Katehi L P B, Ling C C & Rebeiz G M, *IEEE MTT-S Int Microwave Symp Dig*, 2 (1991) 623.
26   Booth J C & Holloway C L, *IEEE Trans Microwave Theory Tech*, 47 (1999) 769.
27   Shen Z Y, *High-Temperature Superconducting Microwave Circuits*. Norwood, MA: Artech House, (1994) 103.
28   Kamenov P, *Superconducting quantum circuits based on disordered aluminum films*, Ph D Thesis, The State University of New Jersey, 2023.
29   Moshe A G, Farber E & Deutscher G, *Appl PhyS Lett*, 6 (2020).
30   Göppl M, Fragner A, Baur M, Bianchetti R, Filipp S, Fink J M, Leek P J, Puebla G, Steffen L & Wallraff A, *J Appl PhyS*, 104 (2008) 113904.
31   Barends R, Vercruyssen N, Endo A, Visser P D, Zijlstra T, Klapwijk T, Diener P, Yates S & Baselmans J, *Appl Phys Lett*, 97 (2010) 023508
32   Wallraff A, Schuster D, Blais A, Frunzio L, Huang R, Majer J, Kumar S, Girvin S, & Schoelkopf R, *Nature (London)* , 431 (2004) 162.
33   Frunzio L, Wallraff A, Schuster D, Majer J & Schoelkopf R, *IEEE Trans Appl Supercond*, 15 (2005) 860.
34   Krupka J, Breeze J, Centeno A, Alford N, Claussen T & Jensen L, *IEEE Trans Microwave Theory Tech*, 54 (2006) 3995.
35   Okasha S & Harada Y, *Int Forum Green Asia*, (2020) 27.
36   Siddiqi I, Verevkin A, Prober D E, Skalare A, Karasik B S, McGrath W R, Echternach P & LeDuc H G, *IEEE Trans Appl Supercond*, 11 (2001) 958.
37   Yanniello B, Aluminum-The other conductor, (Eaton), 2006.
38   Meulenbroeks D, Aluminum versus copper conductors, A white paper issued by Siemens, (Siemens AG) 2014.
39   Pryor L, A comparison of aluminum versus copper as used in electrical equipment, A white paper issued by GE.
40   Schöllhorn C, Zhao W, Morschbach M & Kasper E, *IEEE Trans Electron Dev*, 50 (2003) 740.
41   Queffelec P, Gelin P, Gieraltowski J & Loaec J, *IEEE Trans Magn*, 30 (1994) 224.
42   Patel S M, Kalra Y, V N Ojha V N & Sinha R K, *Indian J Pure Appl Phys*, 56 (2018) 959.
43   Eisenstadt W R & Eo Y, *IEEE Trans Comp Hybrids Manuf Tech*, 15 (1992) 483.